Biophysical and Morphological Evaluation of Human Normal and Dry Eye Meibum Using Hot Stage Polarized Light Microscopy

Igor A. Butovich,[1,2] Hua Lu,[1] Anne McMahon,[1] Howard Ketelson,[3] Michelle Senchyna,[3] David Meadows,[3] Elaine Campbell,[3] Mike Molai,[1] and Emily Linsenbardt[1]

[1]Department of Ophthalmology, University of Texas Southwestern Medical Center, Dallas, Texas
[2]The Graduate School of Biomedical Sciences, University of Texas Southwestern Medical Center, Dallas, Texas
[3]Alcon Laboratories/Novartis, Fort Worth, Texas

Correspondence: Igor A. Butovich, Department of Ophthalmology, University of Texas Southwestern Medical Center, 5323 Harry Hines Boulevard, Dallas, TX 75390-9057; igor.butovich@utsouthwestern.edu.

IAB and HL contributed equally to the work presented here and should therefore be regarded as equivalent authors.

Submitted: September 27, 2013
Accepted: November 14, 2013

Citation: Butovich IA, Lu H, McMahon A, et al. Biophysical and morphological evaluation of human normal and dry eye meibum using hot stage polarized light microscopy. *Invest Ophthalmol Vis Sci*. 2014;55:87–101. DOI:10.1167/iovs.13-13355

Purpose. To study melting characteristics and the morphology of human and mouse meibum.

Methods. Hot stage cross-polarized light microscopy (HSPM) and immunohistochemical approaches were used.

Results. Isolated human meibum, and meibum of mice (either isolated or within the meibomian ducts of mice), were found to be in liquid-crystal state at physiological temperatures. Melting of both types of meibum started at approximately 10°C and was completed at approximately 40°C. Melting curves of isolated meibum and meibum inside the meibomian ducts were multiphasic with at least two or three clearly defined phase transition temperatures, typically at approximately 12 ± 2°C (minor transition), 21 ± 3°C, and 32 ± 3°C, regardless the source of meibum. Melting was highly cooperative in nature. Samples of abnormal human meibum collected from dry eye patients with meibomian gland dysfunction often showed an increased presence of nonlipid, nonmelting, nonbirefringent, chloroform-insoluble inclusions of a protein nature. The inclusions were positively stained for cytokeratins. The presence of these inclusions was semiquantitatively characterized using a newly proposed 0 to 4 scale. In the presence of large amounts of these inclusions, melting characteristics of meibum and its structural integrity were altered.

Conclusions. HSPM is an effective tool that is suitable for biophysical and morphological evaluation of meibum. Morphological properties and melting characteristics of human meibum were found to be similar to those of mice. Abnormal meibum of many dry eye patients contained large quantities of nonlipid, protein-like inclusions, which were routinely absent in meibum of normal controls.

Keywords: hot stage polarized light microscopy, phase transitions, meibomian glands, lipids, biophysics, rheology

Human meibomian glands (MG) are a variant of sebaceous glands[1] that are located inside the tarsal plate of both upper and lower eyelids. Meibomian glands are responsible for supplying meibum, a complex mixture of various lipids that forms the outermost layer of the tear film, called the tear film lipid layer. The major role of this layer is believed to be prevention of evaporation of the aqueous part of the tear film.[2,3] Meibomian glands have secretory acini connected via smaller ductiles to larger and longer, straight central ducts that extend throughout the length of the tarsal plate and open onto the lid margin, close to the posterior lid border, through a number of orifices.[1,4] Each duct is lined with keratinizing stratified squamous epithelium and is similar to epidermis of the skin except for the lack of a granular layer.[5]

Acinar cells in MG vary according to their stage of holocrine differentiation. Three major types of the cells—undifferentiated cells, differentiating cells, and mature or totally differentiated cells—occupy the acini.[6] As the acinar cells differentiate, they start to synthesize and accumulate lipids.[6] The constant production of new meibocytes in the secretory acini, and their disintegration to release the final secretory product, generate a continuous secretory force that drives the meibomian oils within the ductal system of the gland toward the orifice at the free lid margin.[2] Then, all the components of the fully matured acinar cells, including lipids, and (possibly) proteins, nucleic acids, and other types of molecules, are excreted from the orifices and distributed across the ocular surface partly through passive spreading, but largely because of blinking—a concerted motion of upper and lower eyelids—to form the tear film lipid layer.

It has been established that one of the major types of lipids in human meibum is wax esters (WE).[7,8] For a given group of meibum donors (normal, i.e., nondry eye, middle-aged people), variations in the relative lipid composition of meibum did not exceed 10% to 15%.[9,10] Similar observations have been made in three other independent studies.[11–13] Despite sometimes noticeable differences in absolute amounts of individual lipid species and classes reported by these laboratories, all of them reported relatively low interdonor variations in the lipid composition of meibum.

These observations make it reasonable to believe that in normal conditions the chemical composition of meibomian lipids is tightly controlled, and that changes in it may result in tear film instability and cause dry eye–like symptoms.[14–16] Notably, a diet enriched with omega-3 fatty acids did not change the relative posttreatment ratio of detected lipids in human meibum compared to the pretreatment levels.[17]

A wide variety of methods have been used to study the chemical composition of human meibum. These include various types of chromatography (such as gas [GC], liquid [LC], and thin layer chromatography), mass spectrometry (MS), nuclear magnetic resonance spectroscopy, infrared and Raman spectroscopies, and others.[18–20] The most informative are various combinations of GC, LC, and MS approaches used in tandem.[8]

Biophysical evaluation of human meibum requires a different set of tools, among which infrared and Raman spectroscopies have recently gained attention with regard to studying meibum melting and its phase transitions.[18,19] A more traditional way of detecting thermotropic transitions is differential scanning calorimetry (DSC), which was successfully used for human[21] and bovine[22] meibomian lipids. The Langmuir trough technique proved to be very informative for studying meibomian lipid films deposited onto an air–water interface[23–27]: The method has been used for measuring surface-pressure isotherms of meibomian lipids,[28] and, in conjunction with Brewster angle microscopy, for evaluating their topography (the latter approach was pioneered by Kaercher et al.[23,28] for meibum studies).

Another very informative method for studying phase transitions of lipids and lipid mixtures such as meibum is hot stage cross-polarized light microscopy (HSPM). Being able to form liquid crystal-like structures, lipids are capable of producing birefringence patterns in polarized light.[29–34] This feature is helpful for differentiation between lipids and amorphous (i.e., nonbirefringent) nonmelting materials like denatured proteins, which can originate from the cytosol of ascinar cells. Also, by observing and measuring changes in the color of lipid aggregates caused by changes in their temperature, one can detect and study their phase transitions. This approach has been used in a number of studies of other lipid mixtures. Recently, in an industry-sponsored project, HSPM was tested on bovine meibum.[22] In our project (which has been, in part, sponsored by the same entity), we applied HSPM to human and mouse meibum samples and model lipid mixtures. In this paper we refrain from discussing the exact nature (smectic, nematic, and/or cholesteric) of the mesophases of partially melted meibum: The lipid composition of meibum is too complex, and the physical amounts of the material to be analyzed are too small to easily apply standard approaches in an attempt to characterize its properties. However, the more generalized approach that was used in our studies and the results obtained are as follows.

Materials and Methods

Standard lipids used in this study were purchased from Sigma Chemical Co. (St. Louis, MO) and Nu-Chek Prep, Inc. (Elysian, MN). Sodium dodecyl sulfate (SDS), Tween 20, Amido Black, and bovine serum albumin (BSA) were obtained from Sigma Chemical Co. Liquid chromatography and GC/MS grade organic solvents were from various manufacturers. Mouse monoclonal pancytokeratin (PanCK) and rabbit polyclonal anti-cytokeratin 10 (CK10) primary antibodies were from Abcam (Cambridge, MA). Fluorescein-labeled goat anti-rabbit IgG and anti-mouse IgG were from GE Healthcare (Little Chalfont, UK).

To prepare a sample for HSPM analyses, a small amount of a dry standard lipid, a lipid mixture, or human meibum was loaded onto a clean delipidized standard glass slide for microscopy under a Stereomaster microscope (Fisher Scientific, Pittsburgh, PA). Microscopic evaluation of samples was performed using a Nikon Eclipse 50i POL microscope (Nikon Instruments, Inc., Melville, NY) fitted with a Nikon 10×0.25 POL lens, a polarizer, an analyzer, and an LTS420 heating–cooling stage (Linkam Scientific Instruments, Waterfield, UK). Experiments with and without a first-order red tint plate (also known as a compensator) were carried out. Pictures were taken with a Nikon DS-Fi1 color digital camera (equipped with a 2/3-inch image sensor) and processed using Nikon NIS-Elements software. Initially, with no sample or compensator inserted, the analyzer was rotated to a position of maximum extinction of the transmitted light to achieve the darkest background possible. Then, a sample placed on a glass slide was inserted, which caused some light to pass through the optical system because of the anisotropic birefringent nature of the lipid samples. The photographs were captured in a high-quality red-green-blue (RGB) mode as 2560- × 1920-pixel images with a magnification factor of 100 (unless stated otherwise). A typical micrograph of a lipid or an expressed meibum sample taken in this mode and shown in this paper is approximately 1.2 × 0.9 mm (for rectangular pictures) and 0.9 × 0.9 mm for cropped square ones.

To study the melting characteristics of a dry sample, a small amount was loaded onto a glass slide with a microsurgery forceps. Depending on the type of experiment, the sample was either covered with a cover glass or analyzed as is. Then, the slide was inserted in the thermostated LTS420 heating–cooling stage. The heating capability was provided by an electrical heater built into the stage. To cool the sample, the stage was attached to a vacuum flask with liquid nitrogen (Linkam), which was constantly passing cold nitrogen gas through the metal base of the stage. The flow of nitrogen was automatically adjusted with the help of a LN95 liquid nitrogen cooling system that was controlled via a T95-LinkSys PC computer interface and Linksys 32 system controller software (all from Linkam). This setup served dual purposes: (1) The cold vapors of liquid nitrogen allowed us to analyze samples at temperatures below room temperature, and (2) the constant flow of dry gas directed at the glass windows of the stage kept the instrument condensate free. The heating–cooling rate was set to be 2°C/min unless stated otherwise. The heating–cooling experiments were run in cycles. The sample (loaded at room temperature) was initially cooled down to a desired temperature (typically, 10°C–20°C below its phase transition temperature, T_m), and then the sample was gradually heated up until it was completely melted. Then, the temperature of the sample was brought back to the lowest tested temperature, and the cycle was repeated several times. The rates at which samples were cooled and melted were chosen based on the sample type and the design of a particular experiment, and are indicated in the text and legends where appropriate.

The images of the samples at different temperatures were taken and analyzed using the Nikon NIS-Elements software and Adobe Photoshop (Adobe Systems, Inc., San Jose, CA), while computations were performed using Excel (Microsoft, Redmond, WA) and SigmaPlot (Systat Software, Inc., Chicago, IL) software. Exposure times, white balance, gain, and other parameters that influence the pictures were kept constant for each sample to aid the comparison of changes in its birefringence patterns and intensities with the temperature increase or decrease.

The thermotropic crystalline → liquid crystalline → liquid phase transformations of samples were constantly monitored in polarized light for changes in their birefringence patterns

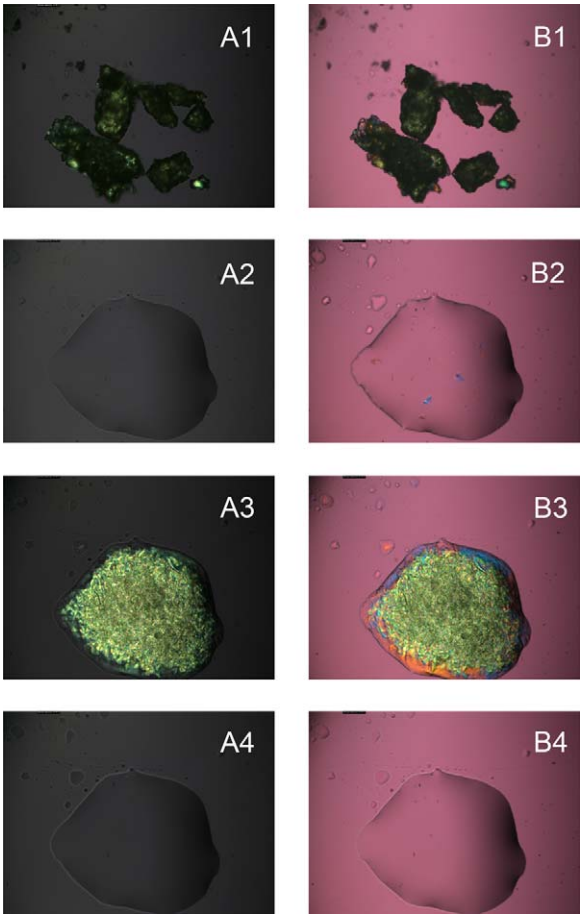

Figure 1. Temperature-dependent changes in the birefringence patterns of a model wax ester behenyl oleate. (**A1–A4**) Observations made in polarized light without the compensator (red tint plate). (**B1–B4**) The same sample was analyzed with the compensator in the light path. Matching photographs of the same sample (**A1–B1**), (**A2–B2**), (**A3–B3**), (**A4–B4**) were taken at matching temperatures by inserting or removing the compensator from the light path. (**A1**, **B1**) Solid sample at 25°C, freshly loaded from the manufacturer's vial. (**A2**, **B2**) Melted sample at 38°C. (**A3**, **B3**) Resolidified sample at 25°C. (**A4**, **B4**) Remelted sample at 38°C. Note that after the first melting–cooling cycle, the footprint and shape of the lipid droplet did not change.

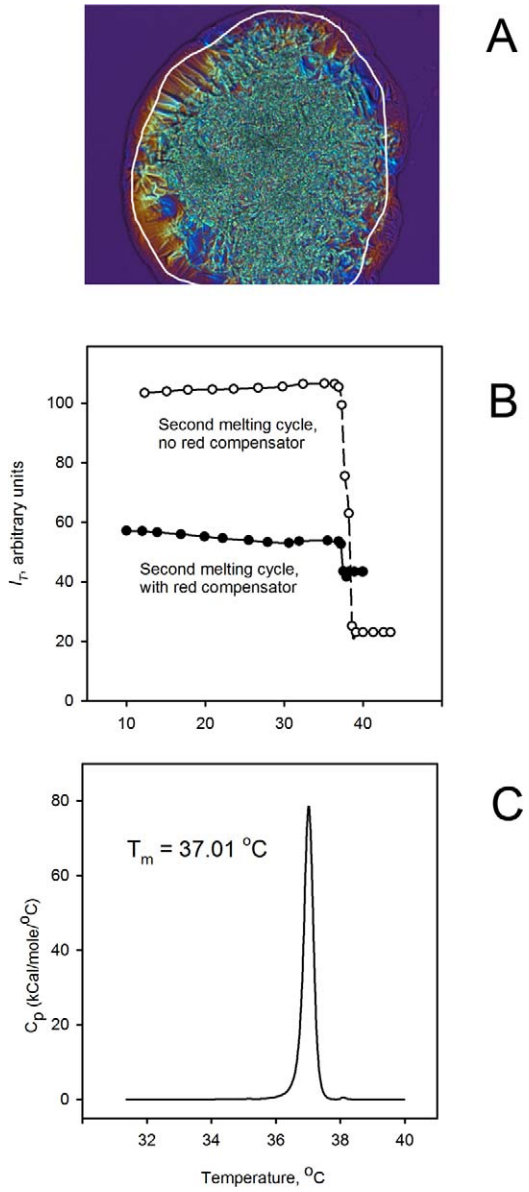

Figure 2. Thermotropic transitions of behenyl oleate. (**A**) Microphotograph of the birefringent patterns of behenyl oleate at room temperature (with the compensator in the light path; microphotographs taken with no compensator are not shown; the appearance of the sample with no compensator inserted was similar to the one shown in Figure 1, A3. (**B**) Melting curves of the lipid obtained without (*upper curve, open circles*) and with (*bottom curve, black circles*) compensator. Note that in this case, due to the initial settings (bright sample, dark background), both curves showed the downward trend. Note that had the background been brighter than the sample, the curve would have shown the upward trend. (**C**) Melting curve of behenyl oleate obtained in a microcalorimetric experiment. Calculated parameters: T_m = 37.01°C; ΔH_{cal} = 25.8 kcal/mol; cooperativity of melting = 58.

and recorded as photo and video files (Fig. 1). Alternatively, still pictures were taken at predetermined temperatures. The use of the red tint plate was optional and depended on the type of experiment (see below). A region of interest (ROI) within a sample was selected in the instrument's RGB channel (as illustrated in Fig. 2A). The values of the intensity of transmitted light detected in the RGB channel within the preselected ROI at different predetermined temperatures were extracted from the data files and exported to Microsoft Excel and then plotted as signal intensity (I_T) versus temperature (T) graphs.

Note that depending on the relative intensities of the background (visible in Figs. 1 and 2 as magenta, uniformly lit areas around the samples) and the sample itself, the extracted I_T versus T graphs may demonstrate either an upward or a downward trend. Both the intensities are proportional to the intensity of the incident light generated by the microscope. To achieve the highest sensitivity, the intensity of transillumination had to be optimized for each kind of sample. If the background was darker than the sample, then the overall brightness of the ROI diminished upon melting. If the background was brighter than the sample, then the intensity of the transmitted light increased with the increase in the sample's temperature. Regardless of the trend, the melting curves were usable for evaluating the values of T_m for each tested sample (see below). Typically, the approach without the compensator in the light path was found to be more sensitive, as the background (with analyzer and polarizer crossed) was typically almost black, and bright birefringent samples were highly visible (Fig. 2B). At the same time, the approach that utilized the compensator provided more information on the

Investigative Ophthalmology & Visual Science

lipid organization within the samples, as anisotropic zones with different directional orders of lipid molecules produced different (mostly yellow, blue, and green) colors easily distinguishable against the magenta background.

Selected samples were evaluated using DSC as described recently.[21] Their thermograms (Fig. 2C) were analyzed to calculate the main transition (melting) temperature T_m, the starting temperature of melting and the ending temperature of melting, cooperative unit size n, van't Hoff enthalpy change, and calorimetric transition enthalpy (ΔH_{cal}).

Cryosections of the eyelid tissues of wild-type mice were prepared as described earlier.[35] The study animals were treated in accordance with the ARVO Statement for the Use of Animals in Ophthalmic and Vision Research. The Nikon microscope's settings were as follows: magnification as indicated in the figure legends (either ×100 or ×400), high-quality RGB mode with image size of 2560 × 1920 pixels. At ×100 magnification factor, the captured image size was 1.2 × 0.9 mm, while at ×400 it was 0.30 × 0.23 mm. The tissue samples (approximately 12 μm thick) were mounted on glass slides. To evaluate the phase transitions of lipids directly in the MG, the slides were placed on the heating stage of the microscope, chilled to 0°C, heated to 50°C or 60°C at a rate of 2 °C/min, and then cooled to 0°C. The cooling–heating cycles were repeated several times to check for reversibility of meibum melting. The changes in the birefringence patterns of meibum within meibomian gland ducts were observed in polarized light both with and without the compensator inserted into the light path. An ROI was selected for each sample individually. Typically, it included the brightest part of the meibomian duct visible in the tissue section. Then, quantitative information on the overall brightness of the ROI (as recorded in the RGB channel) was extracted from the image using the Nikon NIS-Elements software and exported to Microsoft Excel. By plotting I_T versus T, melting curves for meibum within the meibomian ducts were generated. Note that not every tissue section was usable for multiple melting–cooling cycles: Some spreading of lipid material beyond its original location occurred in samples in which tissue apparently had empty spaces for melted meibum to spread to. Thus, many samples could be analyzed only once before spreading occurred.

Our preliminary experiments demonstrated that melting of isolated human meibum could be described using the following model of melting:

$$Crystal(solid, anisotropic, birefringent) \rightarrow$$

$$Partially\ melted\ I(liquid\ crystal, anisotropic, birefringent) \rightarrow$$

$$Partially\ melted\ II(liquid\ crystal, anisotropic, birefringent) \rightarrow$$

$$Melted(fluid, isotropic, non-birefringent)$$

Usually, the values of I_T within preselected ROI were increasing as the samples melted. However, the intensity of the background of the sample needed to be taken into account in each case: If the background was brighter than the sample, the values of I_T were rising, while with a darker background, I_T was diminishing. To determine the values of the three transition temperatures, the data were normalized and then analyzed using a cooperative three-phase transition Hill-type equation (Equation 1) similar to a simpler, one-phase transition equation used previously for analyzing the cooperativity of meibum melting in the dry state and at the air–water interface[21,25,36]:

$$I_T = A + (B \times T^k)/(T_{m0}^k + T^k) + (C \times T^m)/(T_{m1}^m + T^m) + (D \times T^n)/(T_{m2}^n + T^n) \quad (1)$$

The values of starting transmittance (or brightness) of the sample within the preselected ROI (designated as A), three Hill cooperativity coefficients (k, m, and n), relative contributions B, C, and D of the three phase transitions to the overall melting curve, and three phase transition temperatures T_{m0}, T_{m1}, and T_{m2} were computed using a nonlinear fitting routine. Note that the first, lowest-temperature transition was barely detectable in many samples. Thus, in most cases, only two phase transitions T_{m1} and T_{m2} were evaluated.

Without the compensator, the intensity of the transmitted light I_T for any given ROI always changed from high for solidified birefringent samples to low for melted samples. Correspondingly, the extracted I_T versus T graphs showed a downward trend, with numeric values of parameters B, C, and D being negative. The same equation was used to estimate the melting parameters of isolated human meibum.

Clinical Evaluation and Human Meibum Collection and Sample Loading

The study was performed in accordance with the principles of the Declaration of Helsinki. The sample collection procedures were approved by the University of Texas Southwestern Medical Center Institutional Review Board. Two cohorts of patients (totaling 27 volunteers) were recruited. Eighty percent of the participants were recruited from a pool of University of Texas Southwestern Medical Center employees, while the other 20% were recruited by Alcon Laboratories (Fort Worth, TX). Of the 27 volunteers, 5 were normals, while 22 were dry eye patients.

Each of the volunteers recruited at the University of Texas Southwestern Medical Center signed an informed consent form and completed the Ocular Surface Disease Index (OSDI) questionnaire for a standardized evaluation of dry eye–related symptoms. All subjects underwent a thorough anterior segment ophthalmic evaluation. Tear film breakup time and interblink interval were examined, and corneal staining with fluorescein and bulbar conjunctiva staining with Lissamine Green were performed. Both eyes were examined in all subjects. The ocular surface staining was scored according to the standard OSDI protocol. Tear secretion was evaluated using the Schirmer 1 test without topical anesthetics. To evaluate meibum expressibility, the following scale was used: 0, clear, easily expressible meibum; 1, turbid excreta with normal viscosity; 2, turbid excreta with increased viscosity; 3, secretions retained shape after expression; 4, no expressible glands. These data are summarized in Table 1. The details of the meibum collection techniques have been published elsewhere.[36,37]

Chloroform Test and Amido Black Staining of Proteins

The protein content of the samples was evaluated in experiments with Amido Black protein stain. First, a sample of meibum was loaded onto a glass slide. Then, the sample was gently washed with a few drops of chloroform flowing from one side of the sample. The solvent dissolved the lipid material and carried it away from the chloroform-insoluble polar components of the sample. The polar material might have included, for example, proteins, peptides, nucleic acids, saccharides, and inorganic salts. To affix the chloroform-insoluble material to the glass surface, the slide was then incubated at 60°C for approximately an hour. Then, the delipidated polar material was stained with 0.1% Amido Black in a 40% methanol/10% acetic acid solution for 10 minutes, destained twice with 20% methanol in 7.5% acetic acid in water, washed with deionized water, and dried at room temperature. The photographs of the stained

Investigative Ophthalmology & Visual Science

Table 1. Study Samples Collected From Normal and Dry Eye Subjects

	Study Subjects			
	MGD, Total $n = 22$		Normal Controls, Total $n = 5$	
Evaluated Parameters	Males, $n = 7$	Females, $n = 15$	Males, $n = 1$	Females, $n = 4$
Age, y	61.0 ± 8.6	57.8 ± 4.1	53	37.5 ± 3.5
Tear production, mm	8.0 ± 1.3	7.7 ± 0.6	>10	>10
TBUT, s	5.0 ± 1.7	4.5 ± 0.5	>10	>10
Meibum score	1.9 ± 0.2	2.6 ± 0.2	0	0
Cornea stain positive	7	2	0	0
Telangiectasia positive	7	4	0	0
Tear film debris positive, slit lamp	4	1	0	0
Dark, nonmelting, nonbirefringent, nonlipid inclusions in meibum,* range	0–4	0–2	0–1	0–1

TBUT, tear breakup time.
* Evaluated in cross-polarized light using a 0 to 4 grading scheme as described and shown in Table 2.

sample were taken using the Nikon microscope and the digicam.

Immunohistochemistry of Meibum

A sample of intact human meibum was loaded on a positively charged glass slide (Shandon Superfrost Plus; Thermo Scientific, San Jose, CA), washed with ethanol, and placed for 1 hour in an oven preheated to 60°C, after which the slide with the sample was removed from the oven and cooled to room temperature. Then, the slide was hydrated with 1× phosphate-buffered saline (PBS) for 20 minutes and blocked with 10% BSA in PBS at room temperature for 1 hour to prevent nonspecific staining. The slide was incubated with primary PanCK or CK10 antibodies diluted with a 1× PBS buffer with 0.05% Tween 20 overnight in a humidified chamber at 4°C. The slide was rinsed with the buffer three times for 5 minutes each time and then incubated with fluorescein-labeled secondary antibodies diluted in the blocking solution at room temperature for 60 minutes. Then, the sample was rinsed with the buffer three times for 5 minutes each time, and the slide was mounted with aqueous mounting medium.

Results

Birefringence of Pure Lipids and Lipid Standards

When lipid samples were viewed in polarized light, the resulting images showed either bright, lightly colored structures on dark background (without the compensator), or colorful birefringence patterns on a magenta background (with the compensator inserted in the light path; Fig. 1, A1, B1). It was logical to assume that the brightness of the patterns and/or their coloration was proportional to the degree of lipid solidification in the sample. Indeed, melting of initially birefringent samples led to a totally disorganized isotropic liquid lipid material with no birefringence (Fig. 1, A2, B2). Slow cooling the samples caused their solidification/recrystallization (Fig. 1, A3, B3), after which the melting–cooling cycles could be repeated a number of times. The details in the mosaic patterns observed in a series of sequential heating–cooling cycles were never identical, but their overall appearance did not change. Data for behenyl oleate (BO), a representative meibomian wax ester, are shown. Other lipids may display different patterns and/or behavior. Note that after the first heating–cooling cycle, the shape of the lipid droplet stabilized and did not change during subsequent cycles (compare Fig. 1, A2–A4, B2–B4). This behavior was indicative of reversible crystal–liquid crystal–liquid phase transitions of the sample.

From Figure 1, one can see noticeable differences in the brightness of the images of nonmelted and melted samples. Thus, it appeared that these changes could be used to extract information on the melting characteristics of the samples. However, the first melting cycle (shown in Fig. 1, A1, A2, B1, B2), could not be used for this purpose, as the initial irregularly shaped solid particles of lipid samples needed to melt and spread to form a thin layer on the glass slide to become analyzable. Thus, only cycles 2 and above were used to analyze the melting behavior of lipids.

To generate I_T versus T curves, a ROI within a sample (in this case, BO; ROI is the region encompassed by the white line in Fig. 2A) was selected at the beginning of the second melting cycle, and the overall intensity of transmitted light in the RGB channel of the microscope was measured. Then the sample was subjected to melting and, without changing the ROI, its RGB intensity at preselected temperatures was determined. Indeed, when the signal intensity I_T was plotted versus T, melting curves were obtained in experiments without and with the compensator (Fig. 2B). It became evident that the pure lipid melted highly cooperatively in a narrow range of temperatures—the transformation started and ended a few degrees apart (on average, between 35°C and 38°C). Importantly, the temperature range where the changes in the intensity were detected coincided with the temperatures of the main phase transition of BO as measured by differential scanning microcalorimetry (Fig. 2C and Ref. 21).

The morphology of pure lipid samples as seen in polarized light was also evaluated. As a rule, melted and then slowly (0.1°C/min, or less) cooled lipid produced two types of structures with large areas (or macrodomains) of uniform blue and yellow/orange coloration (Fig. 3, white arrows). Also, a third type of lipid aggregation—much more irregular (or granular), greenish-colored zones composed of a very high number of lipid microdomains—was observed, often surrounded by the blue and yellow/orange macrodomains of the sample. These macrodomains seemed to be continuous, each covering a relatively large portion of the sample and overlapping another (Figs. 1–4). One could see that the domains formed three-dimensional sandwiched structures composed of a number of relatively thin sheets positioned on top of each other.

Importantly, the speed of cooling was found to be critical for producing large lipid domains with uniform orientation of molecules—the slower the speed, the larger the domains. The large areas with uniform coloration were routinely observed closer to the edges of the sample, where apparently the sample was thinner, while the more granular zones were found in the central, apparently thicker zones of the samples. Upon cooling

Investigative Ophthalmology & Visual Science

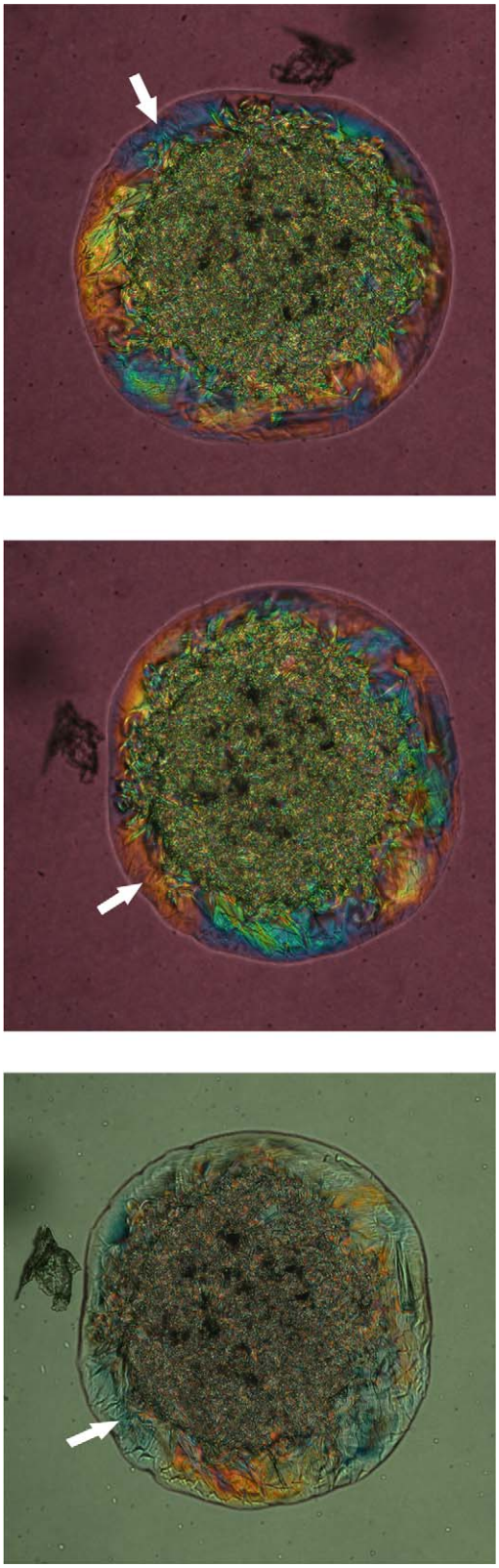

Figure 3. Effects of mutual orientation of the lipid sample, the polarizer, and the analyzer on the birefringence of lipids. (**A**) Initial birefringence of behenyl oleate (polarizer and analyzer are crossed). For clarity, one of the arbitrary chosen lipid domains (initially blue) is marked with a *white arrow*. (**B**) Changes in the birefringence colors of behenyl oleate upon rotation of the sample in the light path of the microscope by 90° counterclockwise (the mutual orientation of optical axes of polarizer and analyzer is not changed). (**C**) The effect of a 90° rotation of the analyzer on the birefringence of the sample. The orientation of the sample is the same as in (**B**). The color of the background changed because of the changes in mutual orientation of the optical axes of the polarizer and the analyzer (they are no longer perpendicular). Note the clearly visible synchronized changes in coloration (*yellow→blue* and *blue→yellow*) of the large, uniformly colored lipid zones at the periphery of the sample. The blue domain that is marked with a *white arrow* in (**A**) turned yellow.

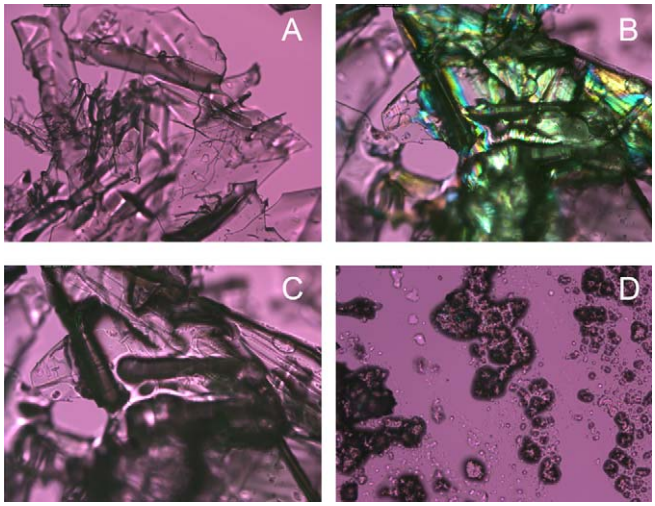

Figure 4. Birefringence of lipid–protein mixtures and the impact of temperature. (**A**) Pure, dry bovine serum albumin has no birefringence. (**B**) Physical mixture of the protein and behenyl stearate at room temperature. Note that only the lipid has birefringence. (**C**) Mixture of the native protein and the lipid at 45°C. The temperature was high enough to melt the lipid, but not the protein, and cause their partial mutual penetration (note visible softening of the edges of the protein crystals in the mixture compared to the sharp edges of the pure protein, and the overall darkening of the sample in the polarized light). (**D**) Mixture of the preliminary denatured/unfolded protein and BS at 45°C. Note that the denatured protein was much more easily mixed with the lipid and formed lipid–protein aggregates similar to those found in abnormal meibum of MGD patients (see below). Magnification: ×100 for all figures.

a melted sample at a rate of 0.1°C/min, crystallization/solidification of a BO sample typically could start anywhere in the sample, eventually spreading to other areas where a thicker lipid phase with granular birefringence patterns formed. The birefringence pattern in the central zone of the sample clearly showed the existence of a large number of microdomains with apparently random orientation of the blue and yellow/orange lipid microdomains (clearly visible in Figs. 1–4), which gave the sample an overall greenish cast. Importantly, crystallization started from the bottom of the samples at the glass–lipid interface, eventually forming large, well-organized layers with uniform blue or yellow coloration, and only later, at lower temperatures, producing smaller and less organized lipid aggregates on top of the thinner but more expansive and ordered lipid domains.

With the compensator inserted, the initially observed birefringence colors changed to the opposite colors (i.e., yellow to blue and blue to yellow) upon rotation of the sample in polarized light (Fig. 3B), or upon rotation of the analyzer (Fig. 3C). Note that the background color also changed because of the changes in the mutual orientation of the optical axes of the polarizer and the analyzer, which was not the case in the experiment shown in Figures 3A and 3B; in that experiment, the mutual orientations of the filters did not

Investigative Ophthalmology & Visual Science

change. Without the compensator, similar manipulations with the sample led to synchronized and repeatable changes in the brightness of various domains of the sample and more subtle changes in its coloration (not shown). Qualitatively similar results were obtained for other tested pure standard lipids. These observations suggested that within each chemically pure WE there were multiple well-organized liquid-crystal nematic and/or smectic mesophases (or domains with different predominant orientations of the lipid molecules).

Effects of Proteins on the Birefringence of Lipids

As MG belong to a group of holocrine glands, their secretions may contain variable amounts of proteins. Despite the fact that most proteins do not mix well with lipids and may become excluded from the lipid phase while in the meibomian ducts, there is a possibility that some of the protein remnants of meibocytes are retained within the meibomian lipid and then expressed onto the ocular surface. This could have an impact on the quality and properties of meibum, the tear film lipid layer, and the tear film in general. The basal levels of proteins in meibum could be affected in certain groups of dry eye patients, such as those diagnosed with meibomian gland dysfunction (MGD) and blepharitis. Thus, we evaluated the effects of proteins on the birefringence patterns of lipid–protein mixtures.

We chose BSA as a model protein, and BO and behenyl stearate (BS) as model lipids. By themselves, particles of pure protein were colorless with no signs of birefringence (Fig. 4A). No changes in the BSA patterns were observed when the samples were heated from 20°C to 70°C. When dry BSA was physically premixed with BO, the protein's physical state did not change. At the same time, the strong birefringence of the lipid was not affected (Fig. 4B). The lipid–protein mixture produced the same types of mesophases (larger zones of uniformly oriented lipid molecules and zones formed from much smaller microcrystals) as the pure lipid samples described above. When the lipid was completely melted (Fig. 4C), no residual birefringence was detectable. Crystallization of different lipid zones of the sample upon its cooling from the melted state appeared to proceed randomly.

An interesting observation was made during these experiments: It seemed that both saturated and unsaturated WE (e.g., BS and BO) had high affinity for the protein as accumulation of BS and BO around the protein particles was observed. It was also noticed that BSA was capable of increasing the T_m of the WE around the protein particles by a few degrees Celsius as the lipid birefringence in the presence of BSA persisted (as bright spots) longer and was gone at higher temperatures than without the protein.

The most dramatic observation was made when BSA had been initially heat denatured in a water–ethanol mixture and then dried, mixed with a chloroformic solution of a wax ester (BO), and dried again. This procedure produced a denatured BSA thoroughly mixed with BO. This mixture was then subjected to repetitive melting–cooling cycles. Interestingly, no transparent, nonbirefringent crystals of BSA were observed: The newly formed dark brown to black material looked amorphous in cross-polarized light. Even more important was the tendency of the denatured protein to retain (or absorb) the lipid within the boundaries of the protein particles: Very little spreading occurred even after heating of the sample to 50°C—well above the melting temperature of BO (Fig. 4D). These observations are discussed later in the paper with regard to MGD meibum.

Finally, it appeared that proteins may have a condensing and/or organizing effect on lipids. This could not be measured directly as the effect was visible mostly within the protein-enriched parts of the samples, which made it difficult to obtain information on the melting curves of the lipid. However, one could see that the lipid retained its birefringence at higher temperatures than the same lipid in the protein-free zones. The increase in the clearing point of the lipid was in excess of several degrees Celsius.

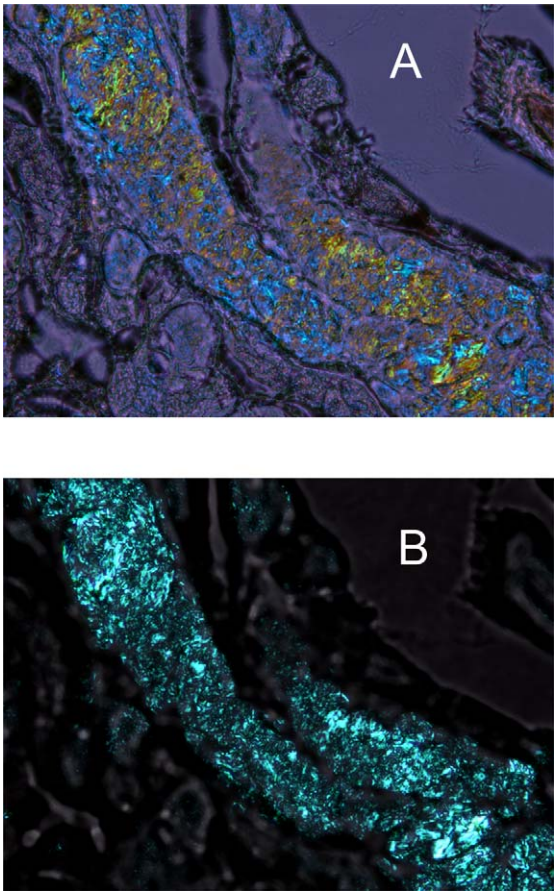

Figure 5. Birefringence patterns of a cryosection of a mouse eyelid at room temperature. (**A**) Mouse meibomian gland as it is seen in cross-polarized light with the compensator in the light path. Note the microgranular structure of the lipid material within the meibomian duct. Different colors (from *yellow* to *blue*) indicate liquid-crystal zones with different predominant orientations of lipid molecules and/or different types of lipids. Magnification: ×400. (**B**) The same cryosection with no compensator. The contrast of the photograph is much higher than that in (**A**), but no conclusions can be made with regard to the presence or absence of zones with different predominant orientations (or directors) of lipid molecules, as no color information is available in this mode. Magnification: ×400.

Birefringence of Mouse and Human Meibum

Tissue cryosections of mouse MG, stained with the lipid stain Oil Red O, demonstrated that their ducts were filled with substantial amounts of meibum.[35] In our current project, the tissue samples were analyzed as is, without the use of the lipid stain. When viewed in polarized light, the lipid content of meibomian ducts showed clearly birefringent patterns (Fig. 5), which confirmed its anisotropic nature. The birefringence was observed both with and without the compensator. The compensator, when inserted into the optical path of the microscope, gave the samples an overall magenta cast and produced colorful liquid-crystal zones within the samples; the majority of the colors were pink, yellow/orange, green, and

Investigative Ophthalmology & Visual Science

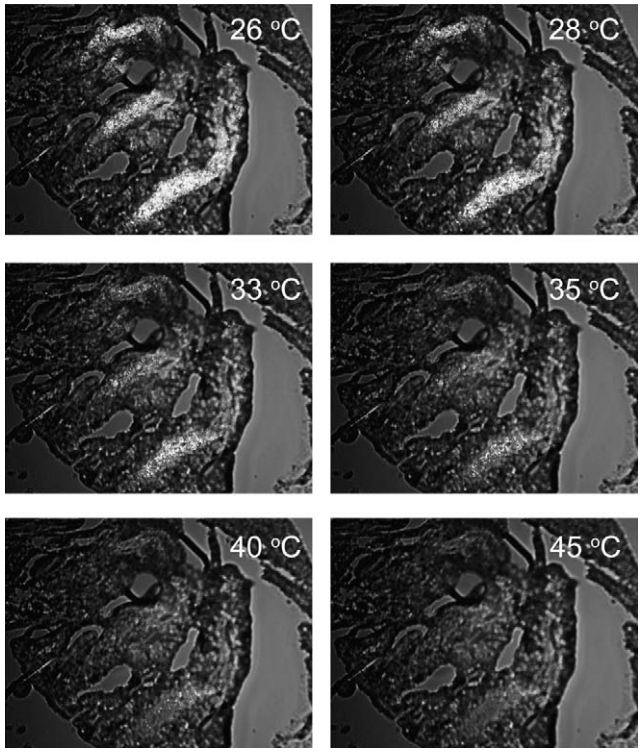

Figure 6. Meibum melting within the meibomian ducts of a mouse. A 12-μm cryosection of a mouse meibomian eyelid was prepared and studied in cross-polarized light with no compensator in the light path. The sample temperatures are indicated in each frame. Note the gradual disappearance of the lipid birefringence with the increase in the temperature of the sample. Most, if not all, birefringence is gone by 40°C to 45°C. After cooling of the sample to approximately 0°C, the birefringence was restored, albeit to a lesser degree than before. We attribute this to spreading of the lipid beyond its original location during the first melting cycle. Magnification: ×100; image size: 0.9 × 1.2 mm.

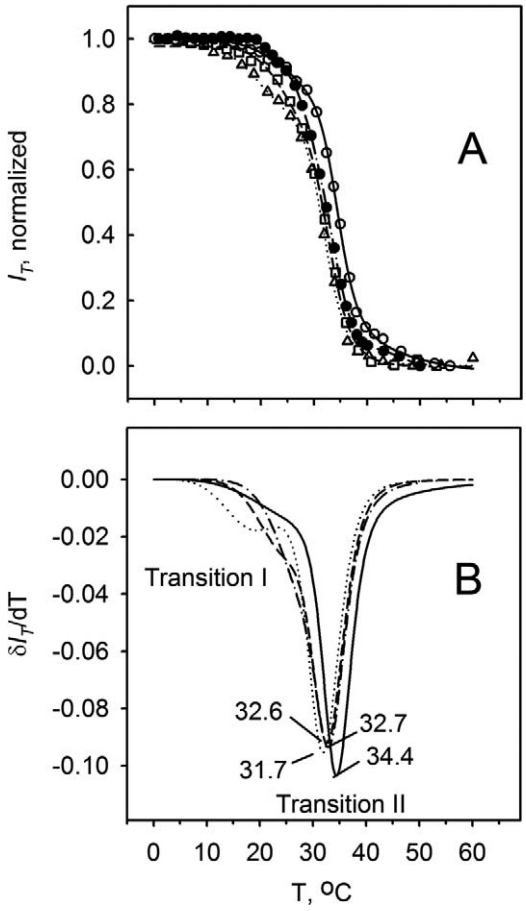

Figure 7. Melting curves of the mouse meibum in the meibomian ducts. Results obtained for four tissue slides from four different mice are shown. No compensator was used. (**A**) Raw melting curves. (**B**) First derivatives of the curves shown in (**A**). Differentiation shows the presence of a shoulder at lower temperatures, which is indicative of an additional phase transition (or pretransition) in the temperature range of 10°C to 25°C.

blue (Fig. 5A). Once the compensator was removed and the analyzer rotated to maximize the contrast of the image (the extinction position), bright white structures on a dark background emerged (Fig. 5B). These changes are typical of anisotropic materials such as various lipid mixtures of artificial and biological origins.[29–34,38]

The microgranularity of the birefringence patterns shown in Figure 5A was indicative of a high degree of inhomogeneity of meibum, since chemically homogeneous samples (such as pure lipid standards) were capable of producing birefringence patterns with much larger areas of uniform coloration.

To determine how birefringence of mouse meibum depended on the temperature, the mouse eyelid cryosections with MG and meibum inside their ducts were subjected to heating with simultaneous monitoring of the changes in the birefringence patterns (Fig. 6). The three bright, elongated structures shown in Figure 6 are the ducts filled with meibum. One can see a gradual temperature-dependent disappearance of the birefringent patterns, with the major change happening between 28°C and 40°C. A very similar transformation was observed with the compensator inserted into the optical path of the microscope (not shown). However, in the latter case the blue, green, and yellow birefringence patterns in the sample disappeared at the end of melting, leaving the sample uniformly pink (with the exception of nonmelting inclusions of nonlipid nature; see below).

It appeared that such a dramatic change in the brightness of the tissue samples could be used to obtain melting curves for the meibum within the meibomian ducts. Indeed, when the samples were analyzed as described and illustrated in Figure 2 for lipid standards, smooth melting curves were generated (Fig. 7). Melting of the meibum within the meibomian ducts started at 10°C to 15°C and was completed at just over 40°C. The major changes in the intensity of the birefringence occurred between 28°C and 40°C. Notably, a 50% change in the I_T for all tested tissue sections was observed between 25°C and 35°C. The curves were successfully analyzed using Equation 1 (Fig. 7A). Two major transition temperatures were detected for the tested tissue samples: The first, slower transition occurred at 23 ± 3°C, while the second, faster one was at 32 ± 2°C. Importantly, the cooperativity of melting (m and n) was found to be approximately 6 for the first, low-temperature transition I and approximately 18 for the high-temperature transition II, respectively.

Subsequent spline approximation and numeric differentiation of the melting curves allowed us to determine at which temperature the samples underwent the fastest transitions (Fig. 7B): It was found that the minima in the corresponding δI_T/dT plots for tested samples were between 31°C and 35°C. Note that after the first melting–cooling cycle, each tissue sample could have been remelted and resolidified several times.

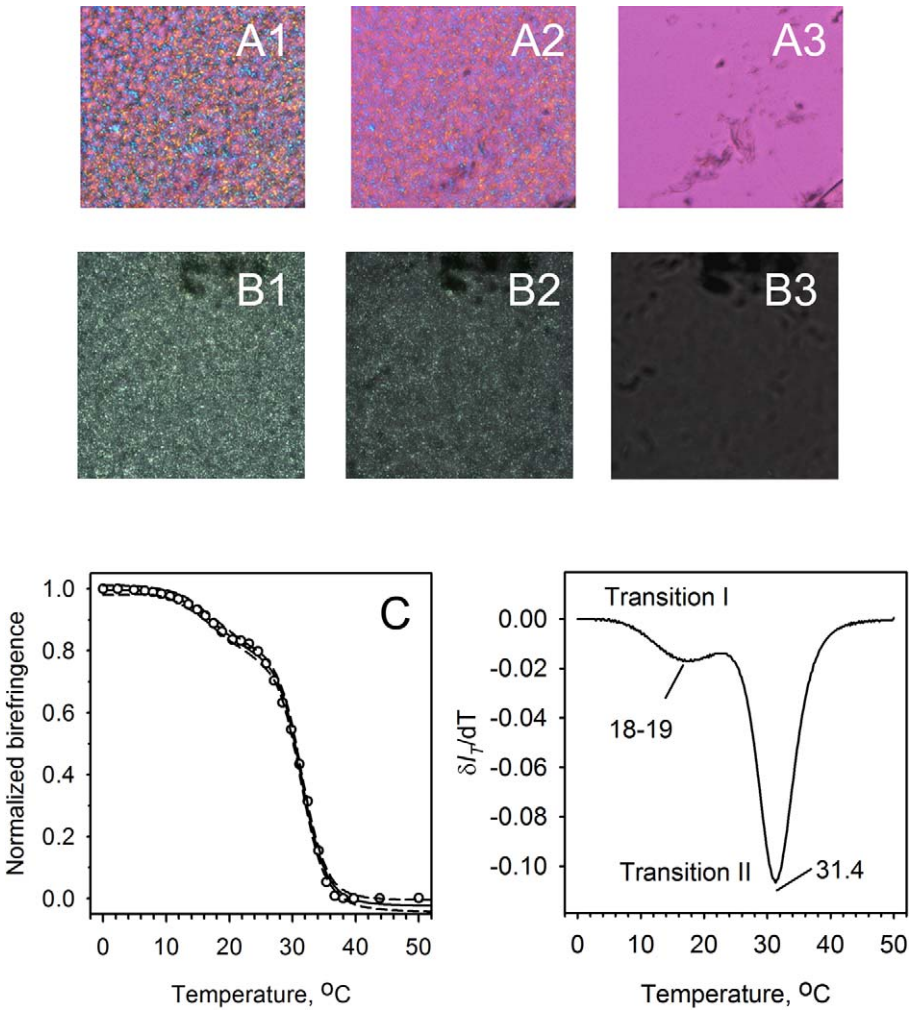

Figure 8. Melting of human meibum. Microphotographs and melting curves of a human meibum sample collected from a donor with mild MGD are shown. (**A1–A3**) Birefringence patterns of meibum with the compensator in the light path taken at three discrete temperatures of 25°C, 32°C, and 40°C, respectively. Note that at a physiological corneal temperature of 32°C, meibum exists in liquid-crystal state. Microgranular lipid domains with different directors are visible as zones with different coloration. Also visible in (**A3**) are nonmelting, nonbirefringent, amorphous dark-colored inclusions, which are imperceptible at lower temperatures. (**B1–B3**) Birefringence patterns of meibum (without the compensator in the light path) taken at 25°C, 32°C, and 40°C, respectively. Note that the inclusions are more difficult to see as they merge with the darker background. However, the changes in the brightness of the sample are greater, which facilitates obtaining quantitative information on its melting characteristics. (**C**) Melting curve of human meibum extracted from the experiment shown in (**B1–B3**). One can see that melting starts at a temperature just below 10°C and is completed at approximately 36°C to 38°C. (**D**) First derivative of the melting curve shown in (**C**). Note the existence of at least two noticeable transitions at around 18°C to 19°C and also at 31.4°C.

However, irreversible changes in the localization of lipids in the meibomian ducts occurred. We found that the overall birefringence of the lipid material diminished with each subsequent heating–cooling cycle due to irreversible spreading of the lipids within the sample beyond their original location within the meibomian ducts. The spreading negatively impacted the sensitivity and accuracy of the analyses. Therefore, the first melting curve for each sample was deemed to be the most representative, while caution was exercised during analysis of its second, third, and subsequent melting curves.

To determine whether isolated mouse meibum melts in a similar way, meibum was expressed from the MG of freshly euthanized mice as described earlier.[35] The size of the samples was found to be too small for a detailed biophysical analysis at this time. However, a limited comparison with the meibum inside the meibomian ducts was possible. We found that the major T_m that was reliably measured for isolated mouse meibum was approximately 32°C, that is, very close to the numbers obtained with the mouse tissue samples.

These observations provided a foundation for further studies of meibomian lipids. As working with tissue samples was not practical in the context of human studies, isolated meibum was tested instead. When human meibum was loaded on a glass slide and then melted and cooled, its birefringence patterns (Fig. 8, A1–A3, B1–B3) emerged. As with mouse meibum, the intensity of birefringence (with no compensator inserted into the light path) changed with temperature, which translated into melting curves (Figs. 8C, 8D). These curves were strikingly similar to those obtained with mouse samples (Fig. 7). Note that the leftmost images (Fig. 8, A1, B1) show the sample in the solid state and the center images (Fig. 8, A2, B2) show the sample's (liquid)-crystal polymorphism, while the rightmost images (Fig. 8, A3, B3) show the isotropic liquid phase with some dark, nonmelting inclusions (see below).

Investigative Ophthalmology & Visual Science

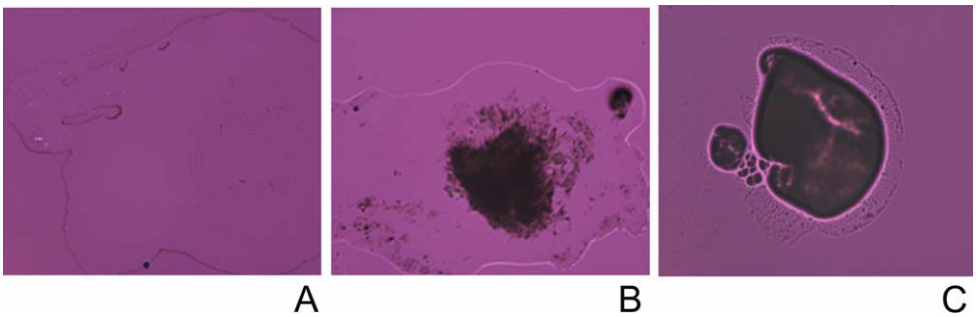

FIGURE 9. Nonmelting, nonbirefringent amorphous inclusions in completely melted human meibum at 40°C. (**A**) Normal, nondry eye meibum. No inclusions are visible. (**B**) Mildly abnormal meibum of a dry eye patient. A moderate amount of inclusions is visible. (**C**) Highly abnormal meibum of a dry eye patient. Lipid component of meibum barely spread beyond the dark, nonbirefringent areas.

The same biphasic transformation as described above for mouse samples was also observed for human samples. To achieve a high correlation coefficient $r^2 \geq 0.998$, only two transitions with two separate transition temperatures T_m were needed. The lower-temperature transition had a T_{m1} of approximately 20 ± 2°C, while the high-temperature transition T_{m2}, which led to the isotropic liquid sample, occurred at approximately 32 ± 2°C. These values were close to the corresponding numbers for the mouse samples, and the temperature of the major phase transition was close to the main phase transition temperatures of approximately 30 ± 1°C for human samples determined earlier in calorimetric experiments.[21] Furthermore, the mean values of m and n for human samples (7 ± 1 and 34 ± 10, respectively; mean ± SD) were of the same order of magnitude as the cooperativity of melting of mouse meibum (see above) and human meibum as tested calorimetrically.[21]

The shapes of the melting curves for some of the tested samples of normal human meibum indicated that there was a third temperature transition involved, which was difficult to observe using the current approach. The T_{m0} of that transition was ≤12°C. However, if it was possible to take the third phase transition into account using a three-phase transition equation with T_{m0} approximately 8°C to 12°C, then the quality of fitting (i.e., the corresponding correlation coefficient r^2) improved from ≥0.998 to ≥0.9998. As this transition typically occurred at very low temperatures and in normal meibum was usually minor, it was difficult to determine its values of T_m, cooperativity, and so on with sufficient accuracy. Moreover, for those curves that could be analyzed using the three-phase transition Equation 1, the inclusion of the lowest-temperature transition into the model did not significantly affect the computed values of T_m, cooperativity coefficients, and so on for the corresponding higher-temperature transitions. For example, the values of T_m and cooperativity coefficients computed using the two approaches differed by just a few percentage points, that is, insignificantly. Also, this lowest-temperature transition occurred at temperatures well below physiological ones. Therefore, it seemed sufficient to use the two-phase transition model for most of the practical needs of the current project, except when an abnormal sample of meibum was encountered (see below).

TABLE 2. Grading System for Meibomian Gland Secretions Based on the Presence of Nonmelting, Nonbirefringent, Nonlipid Inclusions

Meibum Quality	Meibum Grade
Samples with virtually no dark spots/areas	Grade 0
Samples with a negligible presence of dark spots/areas	Grade 1
Samples with a noticeable presence of dark spots/areas	Grade 2
Samples with a large presence of dark spots/areas	Grade 3
Samples predominantly dark, with a small amount of melting material	Grade 4

Normal Human Meibum Versus MGD Meibum

All tested samples of meibum had varying amounts of inclusions (or debris) that did not look like lipids (notice, for example, dark dots in Fig. 8, A3, B3). These inclusions did not melt (i.e., did not become transparent) even in the temperature range from 50°C to 70°C (not shown). In some samples the inclusions were barely detectable, while in others they were a prominent part of the sample.

We found similar-looking, nonmelting, and almost nonbirefringent dark brown to black inclusions in both normal and MGD meibum. It was important to compare the relative amounts of the inclusions in various types of study samples. The inclusions were more readily visible with the red tint plate inserted into the light path. Otherwise, they were virtually invisible due to the generally dark background of the melted samples. This necessitated the use of the red tint plate for comparing the normal and the dry eye samples.

Typically, the quantity of the inclusions was found to be much smaller in normal human meibum than in MGD meibum. Three samples of meibum from three different donors are shown in Figure 9. The tested sample of normal meibum (Fig. 9A) showed only very small amounts of inclusions, while the sample of mild MGD meibum (Fig. 9B) produced visible amounts of dark nonbirefringent inclusions in polarized light. Severe MGD meibum showed the largest amounts of dark inclusions, with a relatively small amount of meltable meibum that surrounded the inclusions. Interestingly, being initially spread all over the sample, the dark material accumulated in the center of the sample once the lipid had been completely melted and became fluid. Similarly to the BSA–BO mixtures described above, the meibomian dark material had a tendency to retain the meibomian lipids, as very little lipid was observed around many samples of melted MGD meibum (Fig. 9C).

The amount of these inclusions in the samples could be described semiquantitatively using the ratio of the area of the melted sample that had inclusions to the total area of the melted sample (note that to correctly estimate the ratio, the whole sample needs to be visible in the microphotograph). Samples were graded according to a 0 to 4 scale (Table 2).

In order to determine if these dark inclusions were lipids or not, the following approach was used. Between 5 and 10 μL chloroform was applied to a meibomian sample affixed to a clean glass slide in an attempt to dissolve the lipid component of meibum and separate it from nonlipid material. These

Investigative Ophthalmology & Visual Science

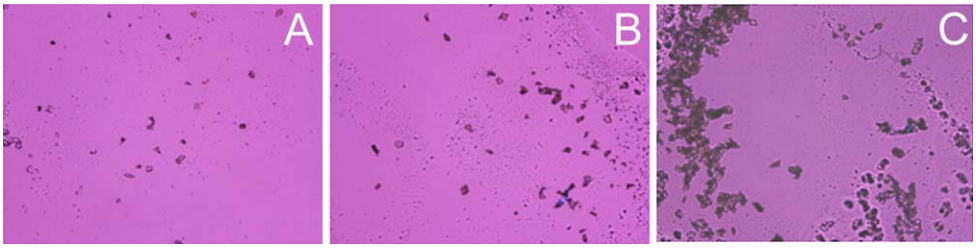

Figure 10. The inclusion bodies in normal (**A**), mild MGD (**B**), and severe MGD (**C**) meibum samples are not soluble in chloroform.

manipulations were monitored microscopically and recorded at the same time. It became clear that the inclusions could not be dissolved in chloroform (Fig. 10). They appeared as off-white to light yellow in color under white light and as dark brown to black largely nonbirefringent particles in polarized light.

These nonbirefringent particles were positively stained for proteins with the nonspecific protein stain Amido Black, and showed reactivity with both PanCK and CK10 antibodies (Fig. 11). The PanCK and CK10 immunostaining pattern of normal human skin scrapings (a positive control) was similar to the staining of human meibum. Immunostaining of wild-type mouse eyelid sections (another positive control) showed CK10 staining in the suprabasal layers of the skin epidermis and in the cells lining the meibomian duct close to the eyelid surface (Fig. 12C). No staining above background was observed in the negative control samples.

Normal and DE meibum samples were melted in HSPM experiments as described above for mouse and normal human samples. Most of the analyzed samples produced typical biphasic sigmoid melting curves. Therefore, two transition temperatures were computed. On average, the first major phase transition in meibum of normal volunteers occurred at T_{m1} of approximately 20 ± 2°C (mean ± SD), the second at T_{m2} of 32 ± 2°C. For dry eye samples the numbers for T_{m1} and T_{m2} were 21 ± 2°C and 33 ± 3°C, respectively. For the reader's convenience, the results are summarized in Table 3. However, some of the melting curves were better approximated using the three-phase transitional model (Fig. 13). Note that the introduction of the third T_{m0} of 9.9°C improved the quality of the fit only at temperatures below 15°C, and did not noticeably change the computed curves at higher, more physiological temperatures. Detailed analyses of the similarities and differences between normal and dry eye meibum, and between different types of dry eye meibum samples, are beyond the scope of this manuscript; these will require a much larger pool of study subjects and will be published separately.

Finally, a potentially important observation was made with regard to the ability of samples of different origin to retain structural integrity under pressure. When a sample of normal meibum was placed on the glass slide, covered with a cover glass, and lightly squeezed in the vertical direction, the sample spread thinly but remained continuous (Fig. 14A). When a similar procedure was performed on samples of meibum from MGD patients, the samples easily disintegrated (Fig. 14B).

Discussion

At a typical corneal temperature of approximately 32°C to 34°C, human and mouse meibum samples are neither completely melted, nor are they crystal-like. Full crystallization of meibum occurs at temperatures well below 10°C, while the secretion enters its completely liquid, disorganized state at temperatures above 40°C. This conclusion, derived from the data obtained using HSPM, is in total agreement with our recently published data on the thermotropic behavior of human meibum evaluated in DSC[21] and Langmuir trough[25–27] experiments, and with our earlier results obtained using a melting point apparatus.[36] It is also corroborated by data published recently by another group[22] that concerned primarily bovine meibum.

The strong birefringence of meibum at all temperatures below 40°C (regardless of whether it is located in a mouse eyelid cryosection or a sample of expressed human meibum) strongly suggests that human meibum exists in a liquid-crystal state at physiological temperatures, as does meibum of mice. The existence of two or three clearly defined phase transition temperatures (and perhaps even more of less visible ones) indicate that meibum undergoes complex phase transitions while melting and/or crystallizing. Importantly, the transitions of both human and mouse meibum start at temperatures of 10°C or so, that is, well below the previously tested range for bovine meibum.[22] At room temperatures of 20°C to 25°C, a substantial part of human and mouse meibum is already melted (Fig. 14), as bovine meibum should be, considering their possible chemical similarities.[7]

Unlike tested pure lipid standards, solid meibum always exists in the form of a very large number of small aggregates (or

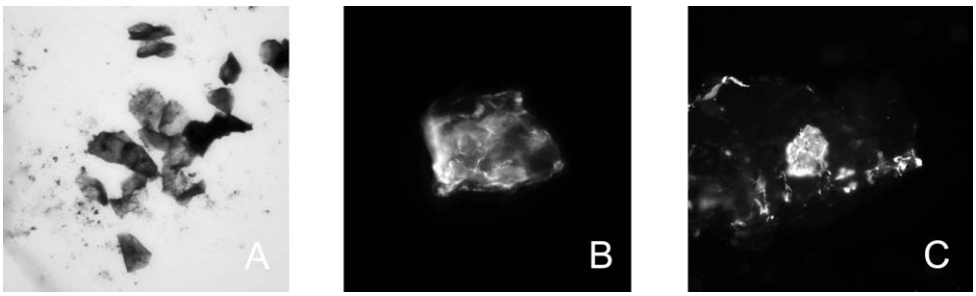

Figure 11. Positive staining of the inclusion bodies with Amido Black (**A**), CK10 antibodies (**B**), and PanCK 10 (**C**) antibodies indicated that they are enriched with proteins, in particular cytokeratins. Microphotographs were taken in white light (**A**) and using fluorescence microscopy (**B**, **C**). Magnification: ×400. Images were cropped to approximately 75 × 75 μm.

Investigative Ophthalmology & Visual Science

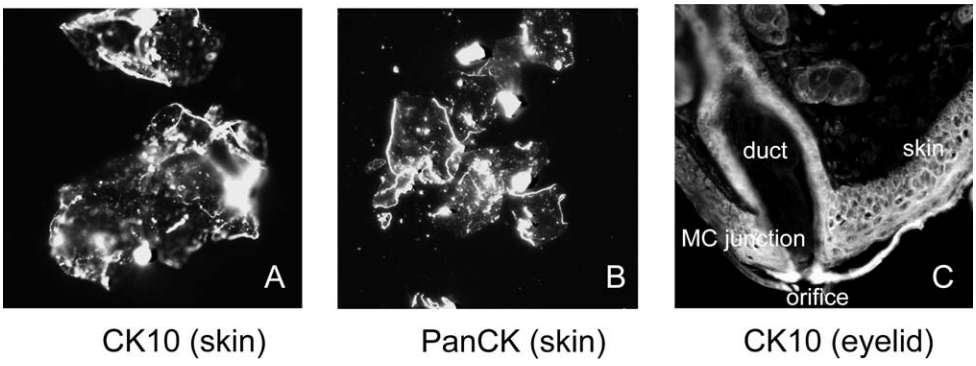

Figure 12. Immunohistochemical anti-CK10 and anti-PanCK staining of particles of stratum corneum collected from human skin and anti-CK10 staining of a tissue section of a mouse eyelid. (**A**) Scrapings of human stratum corneum stained with anti-CK10 antibodies. (**B**) Particles of human stratum corneum stained with anti-PanCK antibodies. (**C**) An OCT-embedded 12-μm cryosection of a mouse eyelid stained with anti-CK10 antibodies. All pictures were taken with a magnification factor of 400 and cropped to approximately 250 × 250 μm.

microcrystals) that produce different colors in cross-polarized light (Figs. 5, 8, 14). The differences in the coloration indicate differences in the preferential orientation of lipid molecules within their respective microdomains. In the tested conditions, meibum never formed large, uniformly colored blue and yellow/orange peripheral areas typical of pure lipid standards (Figs. 1–3). Instead, meibum always demonstrated microgranular patterns similar to those found in the central areas of samples of pure lipid standards. The peripheral areas of pure lipid standards were clearly the zones with uniform orientation of the lipid molecules. The process of self-assembling of the lipids in these zones upon cooling of a completely melted sample always started randomly; that is, the exact location from which the zone propagated and its final shape could not be predicted. However, the central zones of the samples invariantly assumed a heterogeneous state that resembled meibum evaluated in the same conditions. There may be multiple reasons for this physical heterogeneity (in terms of birefringence patterns) of these chemically pure lipid standards (their purity was confirmed to be >99.5% by means of GC/MS). First, crystallization may be initiated by dispersed microinclusions (such as minute dust particles) or imperfections on the surface of the glass slides, all of which can initiate random crystallization of lipids. Second, the thicker central parts of the samples could provide more opportunities for crystals to grow in different directions, thus eventually colliding with other growing crystals with different directors. Third, the glass surface may have an orienting effect on lipid crystallization, favoring a particular orientation of lipid molecules, which is nonexistent in the central parts of the lipid samples that are not in close proximity to the glass.

In sharp contrast with these observations, even the peripheral zones of meibum samples melted/crystallized randomly, and they never produced large, uniformly packed zones. We attribute this to the high chemical heterogeneity of meibum, which consists of hundreds of different lipids.[8] The latter impose considerable diffusion limitations on the crystallization of meibomian lipids and preclude any possibility for them to travel too far because of the high rigidity[25] and viscosity[22,39] of meibum at temperatures below its melting point. Thus, formation of large, chemically homogeneous lipid aggregates of one sort is not possible, and formation of microcrystals of a particular lipid in meibum is stopped once the available pool of proper lipid molecules is depleted in the vicinity of the center of crystallization. This may explain the observed microheterogeneous nature of all tested samples of human and mouse meibum.

The nature of thermotropic transitions (smectic, nematic, and/or cholesteric) was not revealed in our current experiments due to the high complexity of the chemical composition of meibum, its heterogeneity, and the small size of the lipid samples. This will be addressed in future experiments using a range of complementary techniques.

Importantly, the melting transformations of meibum could be followed by monitoring its birefringence, and meaningful and reproducible melting curves could be obtained. As in microcalorimetric experiments, HSPM produced strong evidence that meibum melted cooperatively. The cooperativity

Table 3. Melting Characteristics of Tested Samples

Sample	Average Melting Range, °C (Method)	Transition Temperatures T_m, °C	Cooperativity of Melting
Behenyl oleate	36–38 (microcalorimetry)	37.0 ± 0.2	58
	35–38 (HSPM)	36.0 ± 0.5	49
Mouse meibum in ducts	10–40 (HSPM)	23 ± 3, T_{m1}	6
		32 ± 2, T_{m2}	18
Normal human meibum	10–40 (HSPM)	≤12, T_{m0}	~3
		20 ± 2, T_{m1}	7
		32 ± 2, T_{m2}	34
Dry eye human meibum	10–40 (HSPM)	≤12, T_{m0}	~4
		21 ± 2, T_{m1}	6
		33 ± 3, T_{m2}	38

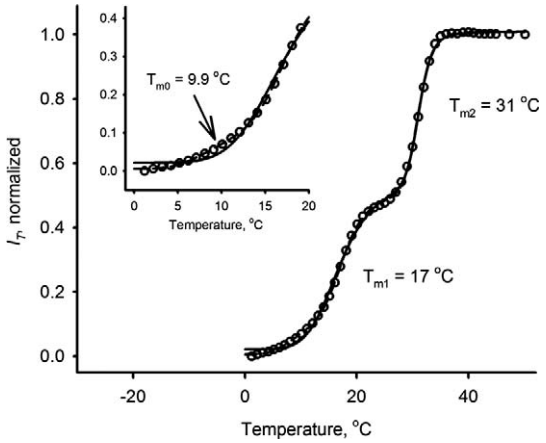

Figure 13. Melting curve of a sample of normal human meibum obtained using the compensator. Two major phase transitions at approximately 17°C and 31°C are clearly visible. A third, lowest-temperature phase transition at approximately 10°C can be observed in the *inset*. The inclusion of this transition in the computational model noticeably improves the quality of approximations for many experiments. However, in some cases the signal-to-noise ratio was not high enough to incorporate this minor transition in calculations.

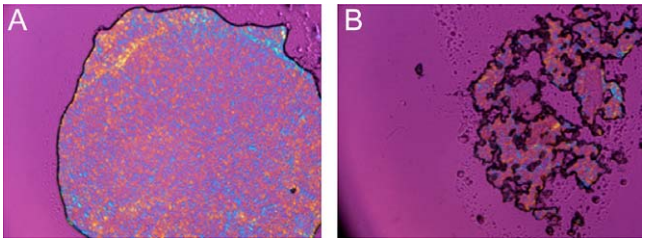

Figure 14. Normal and dry eye meibum differ in their ability to resist mechanical pressure. (**A**) Normal human meibum retained its integrity under mild pressure applied to a sample sandwiched between a cover slip and a glass slide (room temperature). (**B**) In similar conditions, MGD meibum disintegrated under pressure.

coefficients for two clearly visible phase transitions at approximately 20°C and 32°C ($m = 7 \pm 1$, $n = 34 \pm 10$; 5 normal donors; 18 samples) were of the same order of magnitude as the cooperativity measured calorimetrically.[21] Considering that in DSC experiments the measured property of the sample is its heat capacity while in the HSPM it is its birefringence, the closeness of the parameters is extraordinary.

Importantly, the two approaches were in agreement with regard to the melting range of human meibum: Its melting starts at approximately 10°C (i.e., at a much lower temperature than reported recently,[22] but in line with our recent observation[21]) and ends at approximately 35°C to 40°C. Therefore, at a room temperature of approximately 20°C to 25°C and at an average physiological corneal temperature of approximately 32°C, meibum exists in a partially melted, liquid-crystalline state.

Hot stage cross-polarized light microscopy has also been tested for detecting and studying thermotropic phase transitions of meibomian gland secretions in the tissue cryosections of the eyelids of experimental animals (Figs. 5–7). Cryosectioning preserved the lipid material within the MG, a feat that is impossible to achieve when the paraffin embedding technique is used: The solvents used in the latter easily dissolve and/or remove lipids from the ducts. Meibum within the MG was clearly birefringent, that is, in a liquid-crystal state (Figs. 5, 6). The phase transitions of the mouse meibum in the meibomian ducts closely resembled the melting curves of human meibum, with at least two clearly identifiable T_m of 23°C and 33°C, and comparable cooperativities. Note that the amount of meibum that we were able to express from an individual mouse was too low for its detailed characterization by HSPM at this time. With the amount collected, only one, higher-temperature transition at approximately 32°C was detected. This transition was very close to the higher-temperature transition obtained for both mouse tissues and expressed human meibum. Future improvements in the methodology should allow us to conduct more detailed experiments. However, the very fact that one can characterize meibum still within meibomian ducts is encouraging.

As MG are holocrine glands, one can expect that meibum will contain varying amounts of various proteins. It is likely that proteins that might be present in meibum are partially or completely denatured, that is, are unfolded and/or hydrolyzed. Unfolding typically exposes more hydrophobic amino acid residues that otherwise form the hydrophobic cores of intact protein molecules (at least in the case of globular proteins). Therefore, unfolding may increase the overall lipophilicity of the (denatured) protein, making it somewhat more miscible with lipids. To test this hypothesis, we prepared lipid–protein mixtures using BSA in either a native or denatured form. It was found that native BSA mixed poorly with model lipids and tended to retain much of its crystal-like structure (Figs. 4A, 4B). However, the lipid–protein interaction was evident: Once the BSA–BO mixture was comelted, the lipid started to concentrate around the protein crystals, producing a noticeable darkening of the sample due to the formation of diffused, lipid-enriched areas around the protein particles (Fig. 4C).

The most dramatic effect of protein denaturing was observed with predenatured BSA (Fig. 4D): The dark, non-birefringent, diffuse lipid–protein clusters closely resembled those observed in MGD meibum (Fig. 9). Characteristically, the denatured protein seemed to be located within the lipid droplets, having a condensing effect on them, which was indicative of its stronger tendency to interact with lipids. This interaction may be responsible for the observed increase in the melting temperatures of the lipids in the presence of (denatured) proteins. The most immediate physiological consequence of such interactions may be an increase in the melting/transition temperatures of the meibum of patients with an abnormally high presence of protein material in their secretions. It appears that even if the lipid composition of such patients is no different from the norm, the higher presence of (denatured) proteins may cause meibum solidification in the MG and/or ducts, as well as partial or complete stoppage of its flow onto the ocular surface.

Also, considering the tendency of these inclusions to retain lipids (Fig. 9C), they may be responsible, at least in part, for the reduced structural integrity of MGD meibum under physical stress (Fig. 14). One of the possible molecular mechanisms in this case could be the preferential accumulation of amphiphilic lipids around the protein molecules and therefore their depletion in other parts of the sample. This would inevitably lead to lessening of the ability of meibum to interact with hydrophilic surfaces, which is the envisioned primary role of amphiphilic lipids in meibum and the tear film in the first place. Thus, the higher presence of (denatured) protein in certain meibum samples may have a negative impact on meibum properties even if the overall lipid composition of the secretions has not changed.

In line with our experimental observation is a hypothesis that (hyper)keratinization of human MG duct may be associated with various ocular abnormalities, including dry

Investigative Ophthalmology & Visual Science

eye. Jester et al.[40] reported that keratinized epithelium extended throughout the meibomian duct. It has been reported that lid cutaneous hyperkeratinization increases with age and frequently occurs in subjects with telangiectasia.[41] In human skin epidermis, especially in the keratinized cell layers, the most highly expressed cytokeratins are CK1 and CK10.[42] CK10 has previously been detected in the epithelial layer lining the main excretory and intralobular ducts of the mouse MG.[43] In our hands, PanCK- and CK10-specific antibodies strongly stained the wild-type mouse skin epithelium, meibomian gland ducts, and, to a much lesser extent, nonkeratinized tarsal conjunctiva (Fig. 12). One can see that the entire mouse meibomian gland duct epithelium is at least partially keratinized[40,44] and shows a differentiation pattern similar to that of keratinized epidermis.

An important element of our hypothesis is that the amorphous dark inclusions in both normal and MGD meibum (Figs. 9, 10) may have been excess protein derived from keratinized meibomian duct epithelial cells and meibocytes. Our current data demonstrated that the inclusions can neither be melted at a high temperatures (~70°C) nor dissolved in chloroform, which is indicative of their nonlipid nature. Part of the inclusions could be described as semitransparent, nonbirefringent material similar to pure standard proteins, for example, albumin (Fig. 4). These inclusions, but not the meibomian lipids, could be stained with Amido Black, a standard stain for proteins.[45] Most, but not all, inclusions stained positively with CK10- and PanCK-specific antibodies. It was evident that the CK10- and PanCK-positive inclusions existed in both normal and MGD meibum, suggesting that this material may be in part produced by keratinized duct epithelial cells. This corresponds well with the fact that keratins accounted for 25% to 35% of the total proteins in both human and mouse epidermis.[46] The inclusions that we observed in meibum samples collected from normal volunteers and MGD patients (albeit in different amounts) were similar to those reported by Jester et al.[47] for mice with hyperkeratinized ductal epithelium.

Cytokeratin is one of the major parts of the cytoskeleton in epithelial cells. In contrast to healthy living cells,[48] in our samples of meibum, cytokeratin appeared to be mostly in a disorganized/denatured amorphous state with only a small portion of it retaining the filament-like structure. Characteristically, no nuclei were detected, which suggested that the protein material in meibum derived from dead/lysed cells.[49]

Therefore our data, in conjunction with earlier observations, raised the possibility that the nonbirefringent inclusions in both normal and MGD meibum may be of a protein nature, with cytokeratins as prominent components, and may originate from keratinized epithelial cells and meibocytes. It has been demonstrated in independent studies that keratinization of human MG ducts is a normal process.[50] The granular hyperkeratinized material is generally very prominent in MGD subjects (but not in normal controls); this typically is considered a risk factor, as the material can cause blockage of the meibomian ducts with solid hyperkeratinized "plugs." This material can be easily observed in cross-polarized light after sample melting. It is plausible that this granular, nonmelting material could be responsible (at least in part) for the well-known feeling of sandy, or gritty, or foreign body sensation in the eyes—a typical symptom reported by dry eye patients. The newly observed effect of lipid aggregation around the protein particles, as well as a measurable (though variable) protein-induced increase in melting temperatures of such lipid–protein complexes, may be responsible, at least in part, for the increased viscosity, the toothpaste-like consistency, high turbidity, and lower structural integrity of MGD meibum, and can further aggravate the effect of MG plugging. This hypothesis is supported by our observations of MGD meibum and artificial lipid–protein mixtures.

Acknowledgments

Supported in part by National Institutes of Health (NIH) Grant R01EY019480 (IAB), NIH core grant for vision research (EY020799), an unrestricted grant from the Research to Prevent Blindness Foundation (New York, New York), and a grant from Alcon Laboratories (Fort Worth, Texas).

Disclosure: **I.A. Butovich**, None; **H. Lu**, None; **A. McMahon**, None; **H. Ketelson**, None; **M. Senchyna**, None; **D. Meadows**, None; **E. Campbell**, None; **M. Molai**, None; **E. Linsenbardt**, None

References

1. Meibom H. *De Vasis Palpebrarum Novis Epistola*. Helmstadt: Henningi Mulleri; 1666.
2. Mishima S, Maurice DM. The oily layer of the tear film and evaporation from the corneal surface. *Exp Eye Res*. 1961;1:39–45.
3. Rantamäki AH, Wiedmer SK, Hoopainen JM. Melting points – the key to the anti-evaporative effect of the tear film wax esters. *Invest Ophthalmol Vis Sci*. 2013;54:5211–5217.
4. Knop N, Knop E. Meibomian glands. Part I: anatomy, embryology and histology of the Meibomian glands [in German]. *Ophthalmologe*. 2009;106:872–883.
5. Obata H. Anatomy and histopathology of human meibomian gland. *Cornea*. 2002;21(7 suppl):S70–S74.
6. Knop E, Knop N, Millar T, Obata H, Sullivan DA. The international workshop on meibomian gland dysfunction: report of the subcommittee on anatomy, physiology, and pathophysiology of the meibomian gland. *Invest Ophthalmol Vis Sci*. 2011;52:1938–1978.
7. Nicolaides N, Kaitaranta JK, Rawdah TN, Macy JI, Boswell FM, Smith RE. Meibomian gland studies: comparison of steer and human lipids. *Invest Ophthalmol Vis Sci*. 1981;20:522–536.
8. Butovich IA. Tear film lipids. *Exp Eye Res*. 2013;117:4–27.
9. Butovich IA, Uchiyama E, Di Pascuale MA, McCulley JP. Liquid chromatography-mass spectrometric analysis of lipids present in human meibomian gland secretions. *Lipids*. 2007;42:765–776.
10. Butovich IA. Fatty acid composition of cholesteryl esters of human meibomian gland secretions. *Steroids*. 2010;75:726–733.
11. Borchman D, Yappert MC, Foulks GN. Changes in human meibum lipid with meibomian gland dysfunction using principal component analysis. *Exp Eye Res*. 2010;91:246–256.
12. Chen J, Green K, Nichols KK. Quantitative profiling of major neutral classes of human meibum by direct infusion electrospray ionization mass spectrometry. *Invest Ophthalmol Vis Sci*. In press.
13. Lam SM, Tong L, Yong SS, et al. Meibum lipid composition in Asians with dry eye disease. *PLoS ONE*. 2011;6:e24339.
14. Nelson JD, Shimazaki J, Benitez-del-Castillo JM, et al. The international workshop on meibomian gland dysfunction: report of the definition and classification subcommittee. *Invest Ophthalmol Vis Sci*. 2011;52:1930–1937.
15. Joffre C, Souchier M, Grégoire S, Viau S, Bretillon L, Acar N, Bron AM, Creuzot-Garcher C. Differences in meibomian fatty acid composition in patients with meibomian gland dysfunction and aqueous-deficient dry eye. *Br J Ophthalmol*. 2008;92:116–119.
16. Arciniega JC, Nadji EJ, Butovich IA. Effects of free fatty acids on meibomian lipid films. *Exp Eye Res*. 2011;93:452–459.

17. Wojtowicz JC, Butovich IA, Uchiyama E, Aronowicz J, Agee S, McCulley JP. Pilot, prospective, randomized, double-masked, placebo-controlled clinical trial of an omega-3 supplement for dry eye. *Cornea*. 2011;30:308–314.
18. Borchman D, Foulks GN, Yappert MC, et al. Physical changes in human meibum with age as measured by infrared spectroscopy. *Ophthalmic Res*. 2010;44:34–42.
19. Oshima Y, Sato H, Zaghloul A, Foulks GN, Yappert MC, Borchman D. Characterization of human meibum lipid using raman spectroscopy. *Curr Eye Res*. 2009;34:824–835.
20. Shrestha RK, Borchman D, Foulks GN, Yappert MC, Milliner SE. Analysis of the composition of lipid in human meibum from normal infants, children, adolescents, adults, and adults with meibomian gland dysfunction using 1H-NMR spectroscopy. *Invest Ophthalmol Vis Sci*. 2012;53:337–347.
21. Lu H, Wojtowicz JC, Butovich IA. Differential scanning calorimetric evaluation of human meibomian gland secretions and model lipid mixtures: transition temperatures and cooperativity of melting. *Chem Phys Lipids*. 2013;170–171: 55–64.
22. Rosenfeld L, Cerretani C, Leiske DL, Toney ME, Radke CJ, Fuller GG. Structural and rheological properties of meibomian lipid. *Invest Ophthalmol Vis Sci*. 2013;54:2720–2733.
23. Kaercher T, Hönig D, Möbius D. Brewster angle microscopy. A new method of visualizing the spreading of Meibomian lipids. *Int Ophthalmol*. 1993-1994;17:341–348.
24. Schuett BS, Millar TJ. An investigation of the likely role of (O-acyl)ω-hydrohy fatty acids in meibomian lipid films using (O-oleyl)ω-hydroxy palmitic acid as a model. *Exp Eye Res*. 2013; 115C:57–64.
25. Butovich IA, Arciniega JC, Wojtowicz JC. Meibomian lipid films and the impact of temperature. *Invest Ophthalmol Vis Sci*. 2010;51:5508–5518.
26. Arciniega JC, Uchiyama E, Butovich IA. Disruption and destabilization of meibomian lipid films caused by increasing amounts of ceramides and cholesterol. *Invest Ophthalmol Vis Sci*. 2013;54:1352–1360.
27. Georgiev GA, Kutsarova E, Jordanova A, Krastev R, Lalchev Z. Interactions of Meibomian gland secretion with polar lipids in Langmuir monolayers. *Colloids Surf B Interfaces*. 2010;78: 317–327.
28. Kaercher T, Hönig D, Möbius D, Welt R. Morphology of the Meibomian lipid layer. Results of Brewster angle microscopy. *Ophthalmologe*. 1995;92:12–16.
29. Lang PD, Insull W Jr. Lipid droplets in atherosclerotic fatty streaks of human aorta. *J Clin Invest*. 1970;49:1479–1488.
30. Small DM, Shipley GG. Physical-chemical basis of lipid deposition in atherosclerosis. *Science*. 1974;185:222–229.
31. Hata Y, Hower J, Insull W Jr. Cholesteryl ester-rich inclusions from human aortic fatty streak and fibrous plaque lesions of atherosclerosis. I. Crystalline properties, size and internal structure. *Am J Pathol*. 1974;75:423–456.
32. Katz SS, Shipley GG, Small DM. Physical chemistry of the lipids of human atherosclerotic lesions. Demonstration of a lesion intermediate between fatty streaks and advanced plaques. *J Clin Invest*. 1976;58:200–211.
33. Waugh DA, Small DM. Identification and detection of in situ cellular and regional differences of lipid composition and class in lipid-rich tissue using hot stage polarizing light microscopy. *Lab Invest*. 1984;51:702–714.
34. Small DM. George Lyman Duff memorial lecture. Progression and regression of atherosclerotic lesions. Insights from lipid physical biochemistry. *Arteriosclerosis*. 1988;8:103–129.
35. Butovich IA, Lu H, McMahon A, Eule JC. Toward an animal model of the human tear film: biochemical comparison of the mouse, canine, rabbit, and human meibomian lipidomes. *Invest Ophthalmol Vis Sci*. 2012;53:6881–6896.
36. Butovich IA. On the lipid composition of human meibum and tears: comparative analysis of nonpolar lipids. *Invest Ophthalmol Vis Sci*. 2008;49:3779–3789.
37. Butovich IA. Lipidomic analysis of human meibum using HPLC-MSn. *Methods Mol Biol*. 2009;579:221–246.
38. Lundberg B. Thermal properties of systems containing cholesteryl esters and trigycerids. *Acta Chem Scand B*. 1976;30:150–156.
39. Leiske D, Leiske C, Leiske D, et al. Temperature-induced transitions in the structure and interfacial rheology of human meibum. *Biophys J*. 2012;102:369–376.
40. Jester JV, Nicolaides N, Smith RE. Meibomian gland studies: histological and ultrastructural investigations. *Invest Ophthalmol Vis Sci*. 1981;20:537–547.
41. Hykin PG, Bron AJ. Age-related morphological changes in lid margin and meibomian gland anatomy. *Cornea*. 1992;11:334–342.
42. Ming ME, Daryanani HA, Roberts LP, Baden HP, Kvedar JC. Binding of keratin intermediate filaments (K10) to the cornified envelope in mouse epidermis: implications for barrier function. *J Invest Dermatol*. 1994;103:780–784.
43. Lin MH, Hsu FF, Miner JH. Requirement of fatty acid transport protein 4 for development, maturation, and function of sebaceous glands in a mouse model of ichthyosis prematurity syndrome. *J Biol Chem*. 2013;288:3964–3976.
44. Jester JV, Nicolaides N, Smith RE. Meibomian gland dysfunction. I. Keratin protein expression in normal human and rabbit meibomian glands. *Invest Ophthalmol Vis Sci*. 1989;30:927–935.
45. Choveaux D, Krause RG, Goldring JP. Rapid detection of proteins in polyacrylamide electrophoresis gels with Direct Red 81 and Amido Black. *Methods Mol Biol*. 2012;869:585–589.
46. Bowden PE, Quinlan RA, Breitkreutz D, Fusenig NE. Proteolytic modification of acidic and basic keratins during terminal differentiation of mouse and human epidermis. *Eur J Biochem*. 1984;142:29–36.
47. Jester JV, Rajagopalan S, Rodrigues M. Meibomian gland changes in the rhino (hrrhhrrh) mouse. *Invest Ophthalmol Vis Sci*. 1988;29:1190–1194.
48. Pekny M, Lane EB. Intermediate filaments and stress. *Exp Cell Res*. 2007;313:2244–2254.
49. Bragulla HH, Homberger DG. Structure and functions of keratin proteins in simple, stratified, keratinized and cornified epithelia. *J Anat*. 2009;214:516–559.
50. Ong BL, Hodson SA, Wigham T, Miller F, Larke JR. Evidence for keratin proteins in normal and abnormal human meibomian fluids. *Curr Eye Res*. 1991;10:1113–1119.

Investigative Ophthalmology & Visual Science